Tomanikova, L., Savov, I.P., Harvey, J., de Hoog, J.C.M., Churikova, T.G., Gordeychik, B., and Yogodzinski, G.M., 2019, A limited role for metasomatized subarc mantle in the generation of boron isotope signatures of arc volcanic rocks: Geology, https://doi.org. 10.1130/G46092.1.

Supplementary file

PETROLOGICAL DESCRIPTIONS

The mineralogy of mantle xenoliths from Avachinsky (xenoliths found at 53°16'36.0''N and 158°46'38.2''E) and Shiveluch (xenoliths found at 56°33'28.9''N and 161°11'49.2''E) is dominated by olivine and orthopyroxene (spinel harzburgites and dunites; Figure DR1). The harzburgites consist of olivine ($Fo_{90\ to\ 92}$), orthopyroxene (Mg# = 87 to 95) and spinel (Cr# = 50 to 78; Table DR1 and DR2). The dunites consist of olivine (Fo_{88-91}), orthopyroxene (Mg# = 85 to 91) and spinel (Cr# = 59 to 73; Table DR2). Their constituent minerals plot within the same fields as previously studied Avachinsky and Shiveluch mantle xenoliths in the olivine-spinel mantle array (OSMA; Arai, 1992; Figure DR2). Both, the harzburgites and dunites are cross-cut by hydrous metasomatic veins (Figure DR3). Vein cutting through harzburgite *AVX-16-03-10* is monomineralic in the centre, consisting of amphibole (Mg# = 85), and orthopyroxene and clinopyroxene (Mg# = 94.8 and 93.2, respectively) at the contact with the host harzburgite. The vein cutting through harzburgite *AVX-16-03-24* consists of amphibole (Mg# = 94), clinopyroxene (Mg# = 92) and a few grains of phlogopite (Mg# = 94) in the centre and orthopyroxene (Mg# = 92) at the contact with the harzburgite (Figure DR3A). Shiveluch harzburgites *SH98X-16* (Figure DR3B), *SHX03-17* and *SHX03-18* and dunite *SHX03-04* are cross-cut by phlogopite- (Mg# = 85 to 91), amphibole- (Mg# = 80 to 93) and orthopyroxene-rich veins.

Olivine grains in dunite *SHIV-16-12-06* are enclosed in an interconnected network of poikilitic phlogopite (Mg# = 89) throughout half of the sample (Figure DR3C). Chlorite is occasionally present as lamellae within the phlogopite grains.

Shiveluch mantle xenoliths equilibrated at ~ 825 to 942 °C (O'Neill and Wall, 1987; Brey and Köhler, 1990) and 1.3 to 1.7 GPa (Portnyagin and Manea, 2008; Figure DR4). Avachinsky harzburgite *AVX-16-03-10* equilibrated at T ~ 770 °C (Brey and Köhler, 1990)

and P ~ 1.1 GPa (Portnyagin and Manea, 2008). The high Mg# of the constituting minerals and high Cr# of spinels, together with the estimated equilibration P-T, indicate that the mantle xenoliths originated in the upper mantle at 33 to 50 km depth.

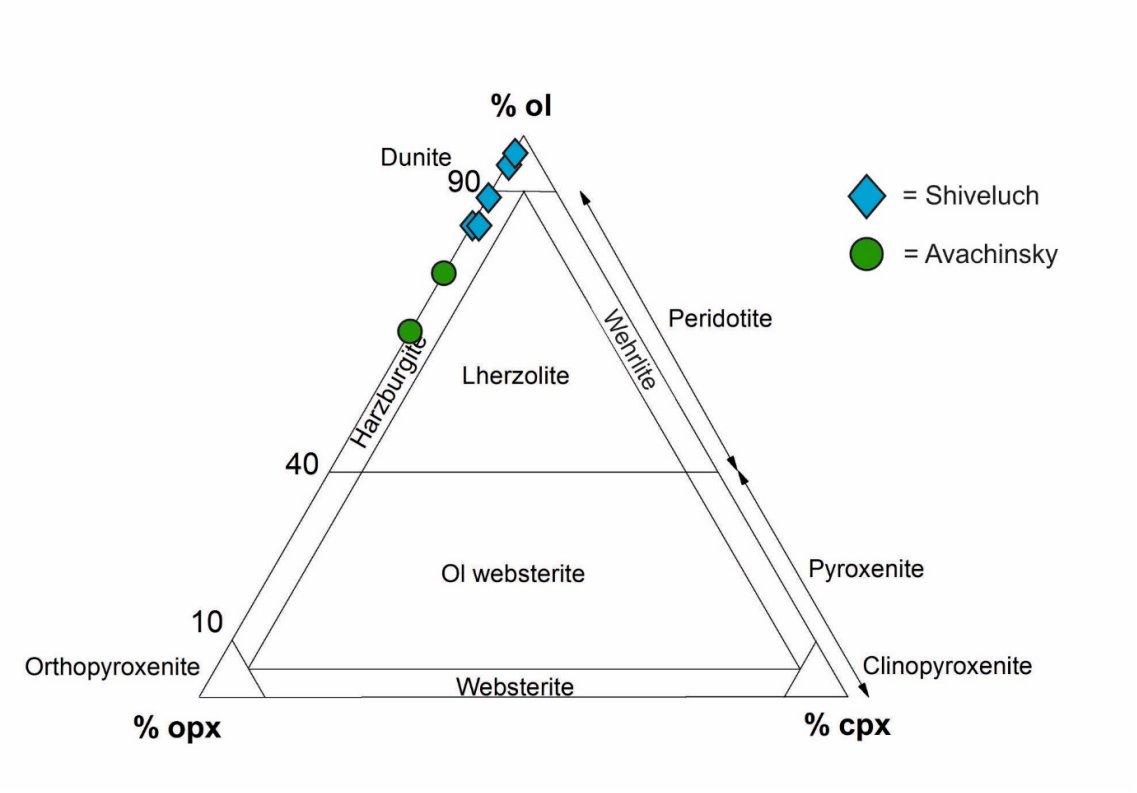

Figure DR1. Classification diagram of mantle xenoliths from Avachinsky and Shiveluch volcanoes (diagram after Streckeisen, 1979 and harzburgite *SH98X-16* and *SHX03-17* from Bryant et al., 2007).

TABLE DR1. MAJOR ELEMENT DATA OF MINERALS IN AVACHINSKY MANTLE XENOLITHS

Sample	AVX-16-03-10					AVX-16-03-24					
Mineral	ol n = 15	opx n = 18	cpx n = 6	spl n = 8	amph n = 36	ol n = 14	opx n = 11	cpx n = 14	spl n = 12	amph n = 33	phl n = 3
SiO_2	40.44	55.75	53.07	bdl	44.10	40.58	56.77	54.11	bdl	50.41	40.09
TiO_2	nd	0.02	0.02	0.08	0.79	bdl	0.01	0.03	0.06	0.05	0.03
Al_2O_3	nd	1.86	1.76	25.27	13.36	bdl	0.87	1.04	14.02	8.39	18.16
Cr_2O_3	0.02	0.33	0.57	38.13	nd	0.01	0.28	0.09	52.36	0.08	0.04
FeO	9.78	6.23	2.37	19.06	7.21	9.92	6.21	2.81	19.53	3.44	2.60
NiO	0.39	0.09	0.05	0.17	0.09	0.39	0.08	0.05	0.06	0.07	0.13
MnO	nd	0.15	0.08	0.20	0.12	0.15	0.15	0.10	0.31	0.06	0.02
MgO	49.21	34.90	18.20	14.91	16.94	49.20	34.42	17.62	11.26	21.13	23.69
CaO	0.11	0.71	24.25	0.12	11.38	0.07	0.63	23.74	bdl	11.79	0.12
Na_2O	nd	nd	nd	nd	2.37	nd	nd	nd	nd	1.31	1.83
K_2O	nd	nd	nd	nd	0.16	nd	nd	nd	nd	0.23	6.27
Cl	nd	nd	nd	nd	0.01	nd	nd	nd	nd	0.01	bdl
F	nd	nd	nd	nd	0.02	nd	nd	nd	nd	0.02	0.01
Total	99.95	100.03	100.36	97.94	96.56	100.31	99.42	99.58	97.61	97.00	91.86
Mg #	89.95	94.80	93.18	67.97	85.27	89.83	91.66	92.16	55.42	94.21	94.16
Cr #	na	na	na	50.32	na	na	na	na	71.50	na	na

Abbreviations: ol = olivine, opx = orthopyroxene, cpx = clinopyroxene, spl = spinel, amph = amphibole, phl = phlogopite, bdl = below detection limit, nd = not determined, na = not applicable.

TABLE DR2. MAJOR ELEMENT DATA OF MINERALS IN SHIVELUCH MANTLE XENOLITHS

Sample	SHX-16-12-06				SHX03-04						SHX03-17					SHX03-18					SH98X-16	
Mineral	ol n = 13	opx n = 10	spl n = 10	phl n = 29	ol n = 6	opx n = 17	cpx n = 5	spl n = 14	amph n = 21	phl n = 4	ol n = 14	opx n = 18	spl n = 10	amph n = 5	phl n = 18	ol n = 9	opx n = 20	spl n = 5	amph n = 17	phl n = 15	amph n = 16	phl n = 17
SiO_2	40.06	54.49	bdl	37.80	40.47	54.01	53.10	bdl	45.12	39.01	41.47	56.96	bdl	53.70	39.79	41.53	56.73	bdl	46.47	39.02	49.25	38.54
TiO_2	nd	0.06	0.70	0.61	bdl	0.04	0.22	0.43	0.67	0.60	bdl	0.01	0.30	0.02	0.11	bdl	0.07	0.34	1.03	1.16	0.47	0.60
Al_2O_3	nd	2.34	10.52	16.88	bdl	0.90	1.11	15.76	10.96	15.37	0.01	0.75	8.48	4.70	15.49	nd	0.41	15.05	10.10	15.94	7.85	16.01
Cr_2O_3	0.02	0.02	42.73	nd	0.26	0.01	0.02	34.25	0.09	0.01	0.13	0.08	46.13	0.02	0.08	bdl	bdl	47.27	0.02	0.01	0.04	0.19
FeO	11.37	8.59	33.42	4.51	9.27	10.77	5.28	35.22	8.12	5.20	8.26	7.34	31.83	3.83	4.20	7.38	8.85	21.45	9.67	6.56	5.62	5.73
NiO	0.21	0.05	0.10	0.12	0.24	0.11	0.10	0.22	0.14	0.41	0.24	0.07	0.12	nd	nd	0.30	nd	0.10	nd	nd	nd	nd
MnO	nd	0.27	0.38	0.02	0.18	0.43	0.22	0.39	0.17	0.04	0.18	0.30	0.42	0.14	0.03	0.14	0.31	0.32	0.19	0.04	0.14	0.03
MgO	48.28	32.56	9.01	21.31	50.47	32.75	17.10	9.82	17.98	24.48	51.09	34.71	9.66	21.99	23.95	52.22	32.28	13.09	16.49	21.56	19.54	22.63
CaO	0.19	0.63	0.12	0.04	0.01	0.43	22.36	0.02	11.01	0.26	0.01	0.17	bdl	11.48	0.04	0.01	0.56	bdl	11.12	0.02	11.90	0.03
Na_2O	nd	nd	nd	2.11	nd	bdl	nd	nd	2.07	0.73	nd	nd	nd	0.88	0.98	nd	bdl	nd	1.89	1.57	1.51	0.95
K_2O	nd	nd	nd	6.28	nd	bdl	nd	nd	0.37	7.27	nd	nd	nd	0.10	8.16	bdl	bdl	nd	0.40	7.07	0.30	8.42
Cl	nd	nd	nd	0.09	nd	nd	nd	nd	0.04	0.07	nd	nd	nd	0.01	0.06	nd	nd	nd	0.02	0.04	0.01	0.03
F	nd	nd	nd	0.10	nd	nd	nd	nd	0.13	0.33	nd	nd	nd	0.11	0.20	nd	nd	nd	0.13	0.27	0.07	0.14
Total	100.12	99.01	96.98	89.87	100.90	99.37	99.51	96.11	96.86	93.77	101.39	100.38	96.94	96.98	93.09	101.59	99.22	97.61	97.52	93.25	96.70	93.31
Mg #	88.31	91.36	44.49	89.41	90.65	85.77	87.52	47.18	85.38	89.27	91.68	91.52	48.29	93.25	91.04	92.65	87.81	62.55	79.57	85.40	89.69	87.54
Cr #	na	na	73.33	na	na	na	na	59.46	na	na	na	na	78.48	na	na	na	na	67.82	na	na	na	na

Abbreviations: ol = olivine, opx = orthopyroxene, spl = spinel, phl = phlogopite, cpx = clinopyroxene, amph = amphibole, bdl = below detection limit, nd = not determined, na = not applicable.

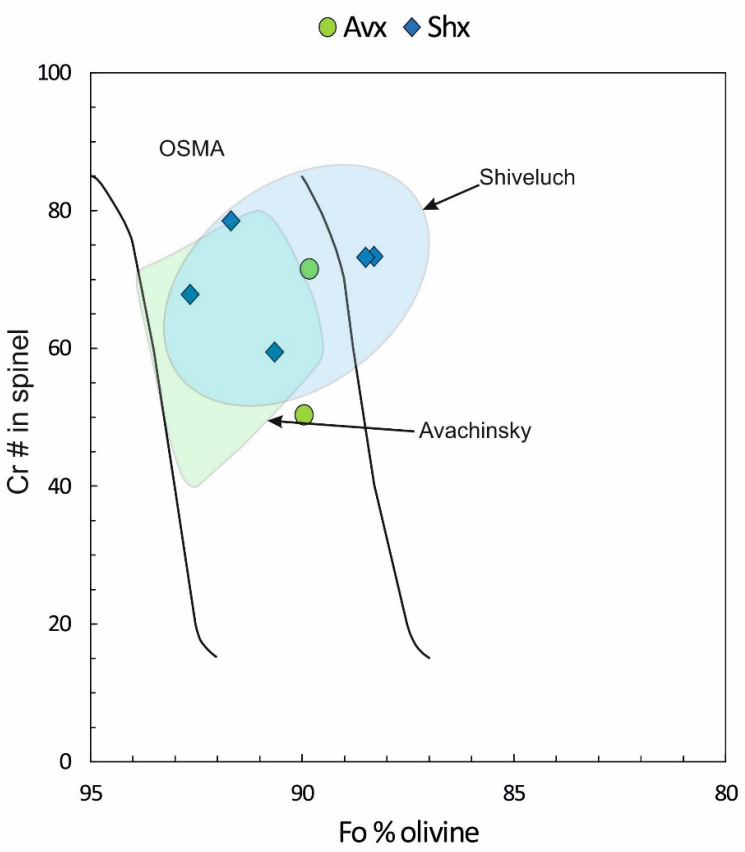

Figure DR2. Spinel Cr# versus average olivine forsterite component of Avachinsky and Shiveluch mantle minerals. Olivine-spinel mantle array (OSMA) after Arai (1992), Shiveluch field from Bryant et al. (2007), Avachinsky field from Kepezhinskas and Defant (1996), Arai et al. (2003), Ishimaru et al. (2007), Halama et al. (2009) and Ionov (2010).

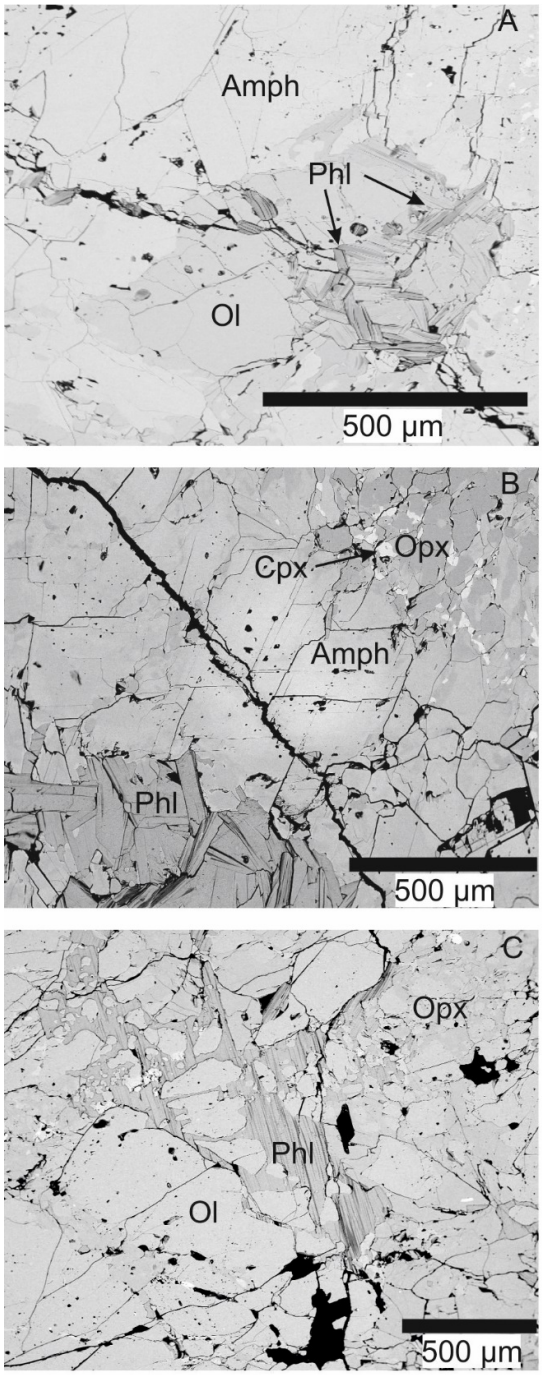

Figure DR3. Back-scattered electron images of hydrous vein minerals in Avachinsky and Shiveluch mantle xenoliths. A) Rare occurrence of phlogopite in a vein cross-cutting Avachinsky harzburgite *AVX-16-03-24*, B) a typical vein consisting of phlogopite and amphibole cross-cutting Shiveluch harzburgite *SH98X-16*, and C) poikilitic phlogopite in Shiveluch dunite *SHIV-16-12-06*.

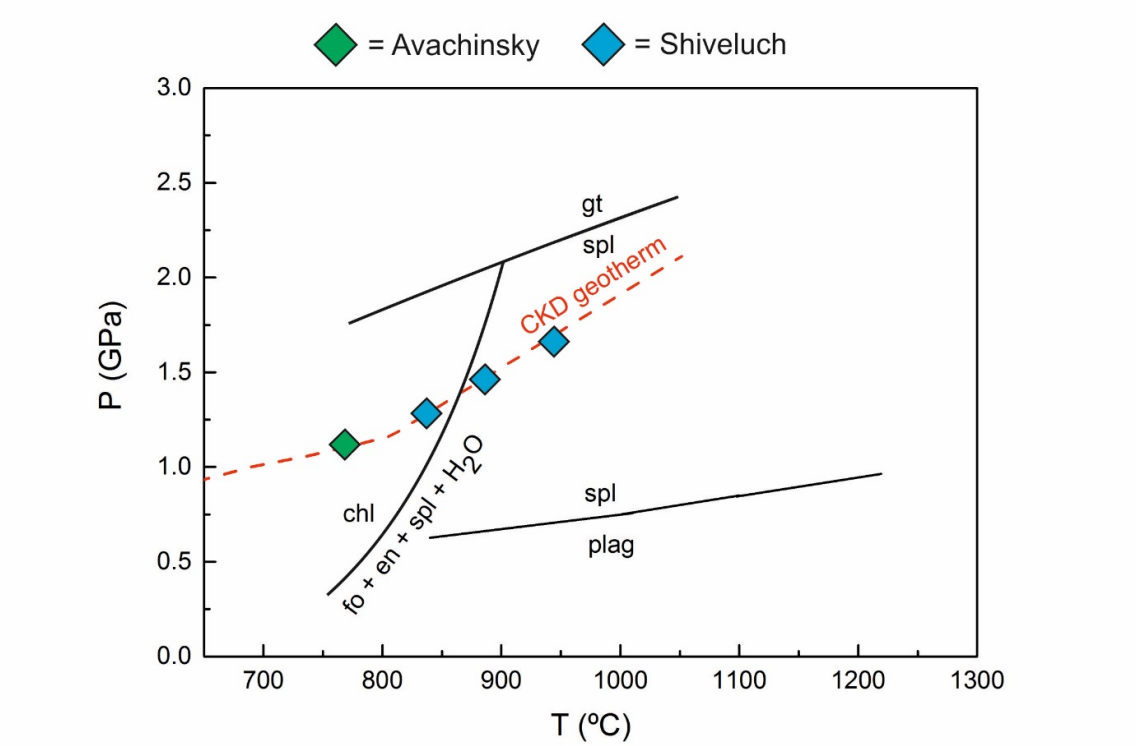

Figure DR4. Equilibration pressure-temperature conditions of Avachinsky and Shiveluch mantle xenoliths. Equilibration temperatures were calculated using two-pyroxene thermometer by Brey and Köhler (1990) and olivine-spinel thermometer by O'Neill and Wall (1987). The CKD geotherm was defined by 23° km^{-1} continental crust thermal gradient and 8.5°C km^{-1} asthenospheric mantle thermal gradient (Portnyagin and Manea, 2008). Chlorite breakdown reaction and garnet-spinel transition is from Ulmer and Trommsdorf (1999) and spinel-plagioclase transition from O'Neill (1981).

REFERENCES

Arai, S., 1992, Chemistry of chromian spinel in volcanic rocks as a potential guide to magma chemistry: Mineralogical Magazine, v. 56, p. 173-184.

Arai, S., Ishimaru, S., and Okrugin, V.M., 2003, Metasomatized harzburgite xenoliths from Avacha volcano as fragments of mantle wedge of the Kamchatka arc: Implication for the metasomatic agent: The Island Arc, v. 12, p. 233-246, doi.org/10.1046/j.1440-1738.2003.00392.x.

Brey, G.P., and Köhler, T., 1990, Geothermobarometry in four-phase lherzolites II. New thermobarometers, and practical assessment of existing thermobarometers: Journal of Petrology, v. 31, p. 1353-1378, doi.org/10.1093/petrology/31.6.1353.

Bryant, J. A., Yogodzinski, G.M., and Churikova, T.G., 2007, Melt-mantle interactions beneath the Kamchatka arc: Evidence from ultramafic xenoliths from Shiveluch volcano: Geochemistry, Geophysics and Geosystems, v. 8, no. 4, doi.org/10.1029/2006GC001443.

Halama, R., Savov, I.P., Rudnick, R.L., and McDonough, W.F., 2009, Insights into Li and Li isotope cycling and sub-arc metasomatism from veined mantle xenoliths, Kamchatka: Contributions to Mineralogy and Petrology, v. 158, p. 197-222, doi.org/10.1007/s00410-009-0378-5.

Ionov, D.A., 2010, Petrology of mantle wedge lithosphere: New data on supra-subduction zone peridotite xenoliths from the andesitic Avacha volcano, Kamchatka: Journal of Petrology, v. 51, no. 1 & 2, p. 327-361, doi.org/10.1093/petrology/egp090.

Ishimaru, S., Arai, S., Ishida, Y., Shirasaka, M. and Okrugin, V.M., 2007, Melting and multi-stage metasomatism in the mantle wedge beneath a frontal arc inferred from highly depleted peridotite xenoliths from the Avacha volcano, southern Kamchatka: Journal of Petrology, v. 48, no. 2, p.395-433, doi.org/10.1093/petrology/egl065.

Kepezhinskas, P., and Defant, M.J., 1996, Contrasting styles of mantle metasomatism above subduction zones: constraints from ultramafic xenoliths in Kamchatka: Geophysical Monograph, v. 96, p. 307-314.

O'Neill, H.St.C., 1981, The transition between spinel lherzolite and garnet lherzolite, and its use as a geobarometer: Contributions to Mineralogy and Petrology, v. 77, p. 185-194, doi.org/10.1007/BF00636522.

O'Neill, H.St.C., and Wall, V.J., 1987, The olivine-orthopyroxene-spinel oxygen geobarometer, the nickel precipitation curve, and the oxygen fugacity of the Earth's upper mantle: Journal of Petrology, v. 28, no. 6, p. 1169-1191, doi.org/10.1093/petrology/28.6.1169.

Portnyagin, M., and Manea, V.C., 2008, Mantle temperature control on composition of arc magmas along the Central Kamchatka Depression: Geology, v. 36, no. 7, p.519-522, doi.org/10.1130/G24636A.1.

Streckeisen, A., 1979, Classification and nomenclature of volcanic rocks, lamprophyres, carbonatites, and melilitic rocks: Recommendations and suggestions of the IUGS subcommission on the systematics of igneous rocks: Geology, v. 7, p. 331-335, doi.org/10.1007/BF01869032.

Ulmer, P., and Trommsdorff, V., 1999, Phase relations of hydrous mantle subducting to 300 km, in Fei, Y., Bertka, C.M., and Mysen, B.O., eds., Mantle petrology: Field observations and high pressure experimentation: A tribute to Francis R. (Joe) Boyd: Special publication no. 6: The Geochemical Society, p. 259.

ANALYTICAL METHODS

Mineral major element abundances were obtained on a JEOL JXA8230 electron microprobe at the University of Leeds. Three different sets of operating conditions were used (Table DR3) dependent on mineralogy.

TABLE DR3. EPMA OPERATING CONDITIONS

Mineral	Accelerating voltage (kV)	Beam current (nA)	Count times major elements (s)	Count times trace elements (s)
Olivine, pyroxenes, spinel	20	30	30	30-45
Phlogopite	20	10	10	30 (Ni), 60 (F and Cl)
Amphibole	20	15	15	30 (Cl), 60 (F)

Primary standards almandine (Al), olivine USNM 2566 Springwater (Si, Mg, Fe), diopside (Si, Mg, Ca), rhodonite (Mn), rutile (Ti), Cr_2O_3 (Cr), Ni metal (Ni) and haematite (Fe), were used to calibrate the mafic mineral analyses.

For phlogopite and amphibole analyses, the primary standards employed were almandine (Al, Fe), diopside (Si, Mg, Ca), rhodonite (Mn), jadeite (Na), K-feldspar (K), rutile (Ti), Ni metal (Ni), fluorite (F) and halite for Cl.

Boron concentrations and $\delta^{11}B$ were measured *in situ* in phlogopite, amphibole, orthopyroxene, olivine and glass using a Cameca IMS-1270 at the Edinburgh Ion Microprobe Facility (EIMF). Boron isotopic compositions are reported as variations in per mil from the boron isotopic standard NIST 951 (boric acid):

$$\delta^{11}B = [(^{11}B/^{10}B_{SAMPLE})/(^{11}B/^{10}B_{NIST\ 951})-1] \times 1000 \quad (1)$$

The primary ion beam of $^{16}O_2^-$ was accelerated to 22.5 kV and impacted upon the sample surface. Beam current steadily increased during the analytical session from 16 to 37 nA and beam size diameter ranged from 20 μm to 30 μm. ^{10}B and ^{11}B signals were detected

sequentially using a single electron multiplier, with counting times of 8s and 2s, respectively, and 100 cycles per analysis. A mass resolution of 2000 (m/Δm) was used to resolve ^{9}BeH and ^{10}BH interferences. Boron concentrations were estimated from ^{11}B count rates using GSD1-G as a standard (50 ppm B). Uncertainties of the B concentrations are ~ 20 % RSD. Amphibole 21664 and 21805, mica MVE02-8-5, 80-3 and JJE01-3 (for phlogopite), serpentine Srp 21826 and Srp-geiss1 and basaltic glass GSD1-G, BCR2-G and pyroxene JJE01-X-3 (for olivine, glass and pyroxene) were used as calibration standards for isotope ratios (De Hoog et al., 2016). Significant matrix effects were observed between different hydrous minerals, as already reported by De Hoog et al. (2016), with offsets of -3.1 ‰, -3.5 ‰ and -4.8 ‰ for amphibole, mica and serpentine compared to basaltic glasses and pyroxene, respectively. Mean relative reproducibility of the δ^{11}B value for the samples was 1.4 ‰ for phlogopite, 1.6 ‰ for amphibole, 1.5 ‰ for orthopyroxene, 1.7 ‰ for olivine and 1.3 ‰ for glass.

REFERENCES

De Hoog J., Monteleone B., Savov I., Marschall H., Zack T. and EIMF, 2017, Matrix effects in B isotope analysis of silicate minerals by SIMS: Goldschmidt Abstracts, 872.

TABLE DR4. BORON CONTENTS AND $\delta^{11}B$ OF VEIN MINERALS IN AVACHINSKY AND SHIVELUCH MANTLE XENOLITHS

Sample	Mineral	B ($\mu g\ g^{-1}$)	$\delta^{11}B$ (‰)	$\delta^{11}B$ 1σ (‰)
AVX-16-03-10	Amph	0.29	-10.28	2.28
		0.37	-9.72	1.79
		0.38	-6.89	1.76
AVX-16-03-20	Amph	0.3 (5)*	-3.60	3.20
AVX-16-03-24	Amph	0.19 (8)	-6.60	3.10
	Phl	0.81	-13.58	1.65
		0.93	-16.65	1.65
SHIV-16-12-06	Phl	2.85	-5.78	0.67
		3.13	-5.01	0.61
		2.99	-6.24	0.59
		2.89	-3.26	0.75
		2.60	-5.37	0.67
		2.64	-3.47	0.68
		2.70	-5.23	0.62
		2.78	-4.85	0.60
		2.80	-4.08	0.63
		1.61	-1.49	0.80
	Ol	0.57	-7.01	1.86
		1.42	-10.26	1.98
		0.82	-4.89	1.38
		0.47	-8.00	1.46
		0.63	-13.84	1.86
SHX03-04	Amph	0.47	-6.46	1.74
		0.93	-10.33	1.15
		1.82	-7.94	0.93
		1.76	-2.54	0.89
	Phl	1.37	-7.79	1.06
		1.05	-9.26	1.09
		1.76	-9.96	0.98
	Gl	0.92	-4.85	1.32
		0.31	-9.08	1.97
		0.97	-7.22	1.36
SHX03-17	Amph	0.92	-7.21	1.67
	Phl	0.76	-10.19	1.68
		1.02	-7.34	1.53
		1.02	-9.89	1.27

		0.67	-8.82	1.81
		0.76	-8.20	1.66
		0.71	-8.31	1.59
	Gl	2.05	-8.88	0.97
SHX03-18	Amph	0.79	-12.13	1.10
		0.51	-9.55	1.07
		0.53	-5.21	1.35
		0.69	-5.85	1.35
		0.38	0.90	1.84
		0.23	-9.02	1.96
		0.27	-4.25	1.65
	Phl	0.73	-11.07	1.16
		0.39	-9.39	1.48
		1.54	-1.90	0.87
		0.30	-4.75	1.97
		0.47	-7.02	1.40
		0.29	-4.96	1.71
		0.31	-5.89	1.73
		0.51	-9.34	1.36
	Opx	0.29	-3.17	2.01
		0.62	-7.64	1.02
	Gl	0.86	-8.97	1.00
		0.33	-13.67	1.55
		0.63	-12.89	1.22
SH98X-16	Amph	0.68	-7.83	1.27
		0.62	-4.68	1.35
		0.58	-5.63	1.64
		0.94	-8.50	1.09
		0.69	-9.68	1.50
		0.54	-1.71	1.54
	Phl	0.27	-4.26	2.35
		0.26	-3.80	2.41
		0.27	-0.53	2.26
		0.28	-6.94	1.87
		0.32	-7.19	1.85
		0.32	-2.61	1.75

Abbreviations: Amph = amphibole, Phl = phlogopite, Ol = olivine, Gl = glass, Opx = orthopyroxene.

*Number of mineral analyses per sample.

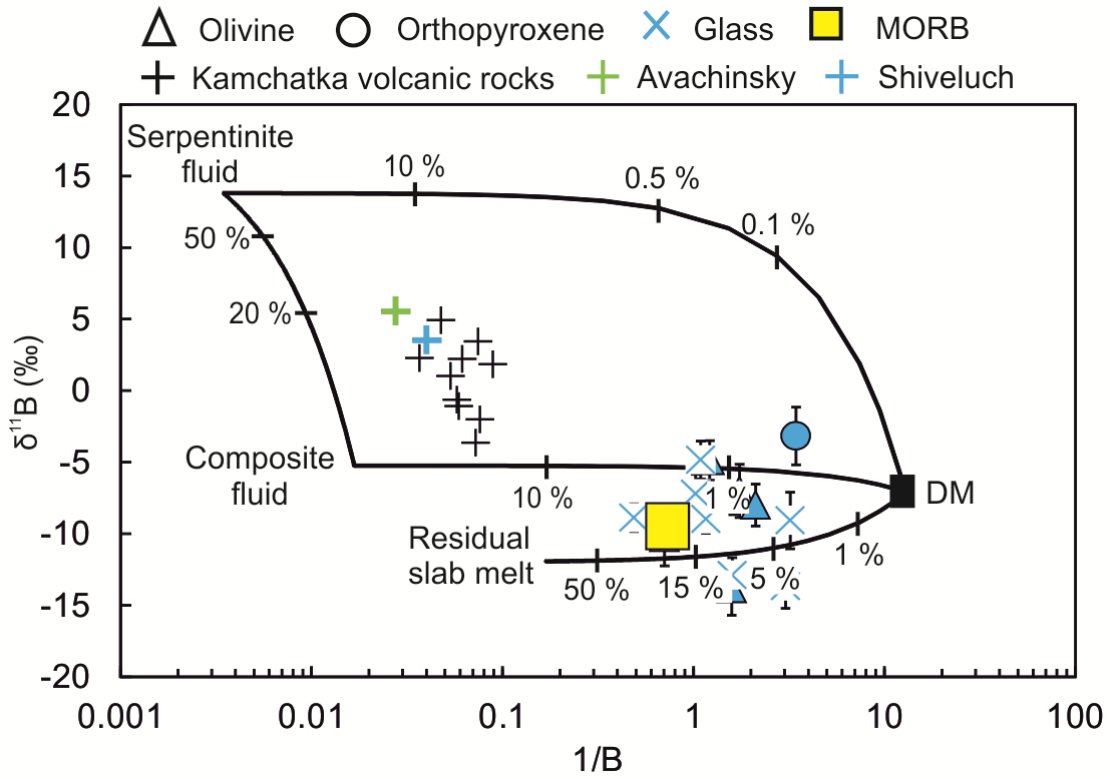

Figure DR5. $\delta^{11}B$ vs 1/B in anhydrous minerals and glass in Shiveluch mantle xenoliths, Kamchatka volcanic rocks (Ishikawa et al., 2001) and MORB (Marschall et al., 2017). The mixing lines between depleted mantle (DM; Marschall et al., 2017), serpentinite fluid (Tonarini et al., 2011) and composite slab fluid are the same as in Figure 2. Please note the lack of B enrichment in the nominally anhydrous minerals relative to MORB. All symbols are larger than the error bars unless shown.

MIXING MODEL

Sources of the hydrous veins were investigated through a B elemental-isotopic mixing model incorporating four mantle B end-members known to date, the depleted mantle (DM; Marschall et al., 2017), serpentinite fluid liberated at 120 depth-to-slab (Tonarini et al., 2011), composite slab fluid comprising altered oceanic crust (AOC)- and sediment-derived fluid and residual slab melt (Table DR5).

TABLE DR5. MIXING MODEL INPUT PARAMETERS

End-member	B ($\mu g\ g^{-1}$)	$\delta^{11}B$ (‰)
DM (Marschall et al., 2017)	0.077	-7.1
Serpentinite fluid released at 120 km depth (Tonarini et al., 2011)	289	+13.8
Composite fluid (calculated after Tonarini et al., 2011)	59.6	-5.2
Residual slab melt (calculated after Tonarini et al., 2011)	5.9	-11.9

Composite fluid comprises 99% AOC-derived fluid and 1% sediment-derived fluid reflecting the maximum estimated sediment proportion of the subducting Pacific plate underneath Kamchatka (Kepezhinskas et al., 1997). Nankai sediment B contents (80 $\mu g\ g^{-1}$) and $\delta^{11}B$ (-4 ‰; You et al., 1997) were used in the calculation of the composite fluid composition and B contents (26 $\mu g\ g^{-1}$) and $\delta^{11}B$ (+5.5 ‰) of the AOC were taken from Leeman et al. (2004). Water contents of Nankai sediments was estimated to be 6.25 wt % (Plank, 2014) and that of the AOC to be 3.7 wt % (Rüpke et al., 2004). Elemental and isotopic B composition of the composite fluid released at 120 depth-to-slab was calculated via a set of mass balance equations after Marschall et al. (2006) under the assumption that B is linked to water release from the subducting lithologies in the slab. The subducting slab was dehydrated at 200 °C, corresponding to the 80 % loss of B in the fore arc (Savov et al., 2007) followed by further slab dehydration at 250, 600 and 650 °C (water loss in sediments with increasing depth of a

cold subducting slab; Rüpke et al., 2004) and finally at 720 °C, corresponding to the AOC water loss under the Kamchatka volcanic arc front (Rüpke et al., 2004; Syracuse et al., 2010).

REFERENCES

Kepezhinskas, P., McDermott, F., Defant, M.J., Hochstaedter, A., Drummond, M.S., Hawkesworth, C.J., Koloskov, A., Maury, R.C., and Bellon, H., 1997, Trace element and Sr-Nd-Pb isotopic constraints on a three-component model of Kamchatka arc petrogenesis: Geochimica et Cosmochimica Acta, v. 61, no. 3, p. 577-600, doi.org/10.1016/S0016-7037(96)00349-3.

Leeman, W.P., Tonarini, S., Chan, L.H., and Borg, L.E., 2004, Boron and lithium isotopic variations in a hot subduction zone-the southern Washington Cascades: Chemical Geology, v. 212, p. 101-124, doi.org/10.1016/j.chemgeo.2004.08.010.

Marschall H.R., Ludwig, T., Altherr, R., Kalt, A., and Tonarini, S., 2006, Syros metasomatic tourmaline: Evidence for very high-δ^{11}B fluids in subduction zones: Journal of Petrology, v. 47, no. 10, p. 1915-1942, doi.org/10.1093/petrology/egl031.

Marschall, H.R., Wanless, V.D., Shimizu, N., Pogge von Strandmann, P.A.E., Elliot, T., and Monteleone, B.D., 2017, The boron and lithium isotopic composition of mid-ocean ridge basalts and the mantle: Geochimica et Cosmochimica Acta, v. 207, p. 102-138, doi.org/10.1016/j.gca.2017.03.028.

Plank, T., 2014, The chemical composition of subducting sediments, in Holland, H., and Turekian, K., eds., Treatise on Geochemistry: Volume 4: Elsevier Ltd., 607 p.

Rüpke, L.H., Morgan, J.P., Hort, M., and Conolly, J.A.D., 2004, Serpentine and the subduction zone water cycle: Earth and Planetary Science Letters, v. 223, p. 17-34, doi.org/10.1016/j.epsl.2004.04.018.

Savov, I.P., Ryan, J.G., D'Antonio, M., and Fryer, P., 2007, Shallow slab fluid release across and along the Mariana arc-basin system: Insights from geochemistry of serpentinized

peridotites from the Mariana fore arc: Journal of Geophysical Research, v. 112, doi.org/10.1029/2006JB004749.

Syracuse, E.M., van Keken, P.E., and Abers, G.A., 2010, The global range of subduction zone thermal models: Physics of the Earth and Planetary Interiors, v.183, p. 73-90, doi.org/10.1016/j.epsl.2015.07.031.

Tonarini, S., Leeman, W.P., and Leat, P.T., 2011, Subduction erosion of forearc mantle wedge implicated in the genesis of the South Sandwich Island (SSI) arc: Evidence from boron isotope systematics: Earth and Planetary Science Letters, v. 301, p. 275-284, doi.org/10.1016/j.epsl.2010.11.008.

You, C.-F., Chan, L.H., Spivack, A.J., and Gieskes, J.M., 1995, Lithium, boron, and their isotopes in sediments and pore waters of Ocean Drilling Program Site 808, Nankai Trough: Implications for fluid expulsion in accretionary prisms: Geology, v. 23, no. 1, p. 37-40, doi.org/10.1130/0091-7613(1995)023<0037:LBATII>2.3.CO;2.